



A machine learning model for flank wear prediction in face milling of Inconel 718

Tiyamike Banda¹ · Yu-chen Liu^{2,3,4,5,6} · Ali Akhavan Farid¹ · Chin Seong Lim¹

Received: 1 November 2022 / Accepted: 23 February 2023 / Published online: 4 March 2023
© The Author(s), under exclusive licence to Springer-Verlag London Ltd., part of Springer Nature 2023

Abstract

Optimization of flank wear width (VB) progression during face milling of Inconel 718 is challenging due to the synergistic effect of cutting parameters on the complex wear mechanisms and failure modes. The lack of quantitative understanding between VB and the cutting conditions limits the development of the tool life extension. In this study, a Gaussian kernel ridge regression was employed to develop the VB progression model for face milling of Inconel 718 using multi-layer physical vapor deposition-TiAlN/NbN-coated carbide inserts with the input feature of cutting speed, feed rate, axial depth of cut, and cutting length. The model showed a root mean square error of 30.9 (49.7) μm and R^2 of 0.93 (0.81) in full fit (5-fold cross-validation test). The statistics along with the cross-plot analyses suggested that the model had a high predictive ability. A new promising condition at the cutting speed of 40 m/min, feed rate of 0.08 mm/tooth, and axial depth of cut of 0.9 mm was designed and experimentally validated. The measured and predicted VB agreed well with each other. This model is thus applicable for VB prediction and optimization in the real face milling operation of Inconel 718.

Keywords Machine learning · Flank wear prediction · Optimization · Inconel 718

1 Introduction

Inconel 718 constitutes more than 50% of modern aircraft engines' structural components [1]. Due to its superior properties, such as creep, oxidation, hot corrosion resistance, and

high hot hardness, it withstands vigorous operating conditions in high-temperature engine cores [2]. The machining process for Inconel 718 includes drilling, face milling, and turning. Among the all, face milling is known for a high-quality surface finish, producing more precise components for very minimal dimensional tolerance applications [3]. However, the typical machinability rating of Inconel 718 is between 0.09 and 0.3, which is less than 0.4, 1.2, and 1.9 for stainless steel 304, Al 6061, and 7075 alloys, respectively [4]. Hence, Inconel 718 is considered a hard-to-machine Ni-based alloy because of the high affinity to form a built-up edge (BUE), to react with tool's elements, and to undergo precipitation hardening [5]. Such complex metallurgical properties facilitate tool wear mechanisms, which mainly include adhesion, abrasion, diffusion, and oxidation [6]. These mechanisms cause rapid tool deterioration, covering a spectrum of damage scales from micro-chipping to gross fracture [7]. More details of wear mechanisms and failure modes during face milling of Inconel 718 have been pursued in Ref. [8]. Flank wear is considered a dominant failure mode that determines the tool life when face milling Inconel 718, and is primarily caused by the abrasion wear mechanism [9]. It evolves in three stages, namely early rapid wear, uniform wear, and failure region [10]. The unprecedented

✉ Yu-chen Liu
ycliu19@gs.ncku.edu.tw

¹ Department of Mechanical, Materials and Manufacturing Engineering, University of Nottingham Malaysia, Semenyih, Malaysia
² Department of Mechanical Engineering, National Cheng Kung University, Tainan 70101, Taiwan
³ Hierarchical Green-Energy Materials (Hi-GEM) Research Center, National Cheng Kung University, Tainan 70101, Taiwan
⁴ Program On Smart and Sustainable Manufacturing, Academy of Innovative Semiconductor and Sustainable Manufacturing, National Cheng Kung University, Tainan 70101, Taiwan
⁵ Program On Semiconductor Packaging and Testing, Academy of Innovative Semiconductor and Sustainable Manufacturing, National Cheng Kung University, Tainan 70101, Taiwan
⁶ Core Facility Center, National Cheng Kung University, Tainan 70101, Taiwan

failure modes in the failure region, such as chipping, flaking, BUE, and notching, affect the surface finish and dimensional tolerance of the components. As such, an optimal face milling process allows flank wear retaining in the uniform region and minimizes these unprecedented failure modes. The uniform flank wear width (VB) ranging between 200 and 500 μm is thus considered minimum and maximum tool life, as presented by ISO 8688–1 standard.

Currently, the modern multi-layer-coated tools are widely applied to avoid rapid VB progression because they have a high hardness, elastic modulus, and plasticity [11], and thus replace uncoated or single-layered coated tools [12]. The multi-layer-coated inserts with fine-crystalline TiAlN primary layers are known for Inconel 718 face milling operation [13]. On top of that, cutting condition optimization is a key to achieve the highest tool performance [14]. Research suggested that parameters of the cutting speed, feed rate, and axial depth of cut (ADOC) significantly affect tool performance in the Inconel 718 face milling operation [15]. Nevertheless, these parameters have synergistic effect to VB [16]. Owing to the lack of the physically based mathematical correlation between the cutting parameters and VB, modulating these parameters via empirical methods is time-consuming and costly [17]. It is thus necessary to build up a model to predict VB progression in order to avoid unprecedented tool failure.

Indirect tool condition monitoring (TCM) uses sensors to collect tool wear data during machining [18, 19]. This data is then analyzed using techniques such as statistical analysis, wavelet transform, and time–amplitude analysis, to extract features that correlate with VB progression. For example, Gao et al. [20] used wavelet transform to convert force signals into more sensitive statistical features that accurately reflected wear states. On the other hand, direct TCM methods use machine and computer vision technology to acquire and extract geometric, textural, and fractal features [21]. These features are then combined with process parameters to develop predictive models, such as fuzzy logic, and regression analysis [22]. However, the combined effect of various process parameters on failure modes can result in multicollinear data, making it difficult for predictive models to accurately extrapolate VB progression under unknown processing conditions and with limited training dataset. This can lead to classical models performing poorly or failing altogether during TCM.

Recently, deep learning (DL) and machine learning (ML) model are considered powerful methods to decipher and explore the complex underlying physics of the materials science and engineering [23], including quality prediction in manufacturing [24], effective charge in electromigration effect [25], dielectric constant and dissipation factor in low-temperature co-fired ceramics [26], and irradiation embrittlement in steel [27]. More relevantly, direct tool wear

detection of physical vapor deposition (PVD)–coated carbide inserts by using a convolution neural network (CNN) model using image features is one of the approaches to characterize failure occurrence [28]. In pursuing a direct VB prediction during facing milling, Kaya et al. [29] applied an artificial neuron network (ANN) model to predict VB of single-layered PVD-TiAlN coated inserts (i.e., R390-11 T3 08 M-PL 1030) using the input features of cutting speed, feed, ADOC, time, force, and torque of a 5-axis CNC milling center. The model achieved a correlation coefficient (R^2) of 0.99, and a mean relative error of 5.42% in testing the validation data set not used in fitting the model. Although it is shown that ML method is applicable in predicting VB, the model was built based on data where a single-layer-coated tool was used. To the best of the authors' knowledge, there have been very few studies in developing VB prediction model using ML methods for PVD-multi-layer-coated inserts during face milling of Inconel 718. On the other hand, the existing physically based models can neither decipher the underlying curvature of VB progression nor design better cutting conditions to minimize rapid tool failure [30]. Therefore, this research focuses on developing a ML model to extrapolate the VB progression of multi-layer PVD-TiAlN/NbN-coated carbide inserts during face milling of Inconel 718. Unlike the NN-based models presented in previous research, the ML model used in this work was the Gaussian kernel ridge regression (GKRR) model, which is powerful in predicting unknown data with the information of the vicinity data in the training data set, to predict the VB progression. In addition, less hyperparameters are used in GKRR than conventional NN-based models, and therefore would help to eliminate overfitting issue over a small dataset and in the meantime speed up the training process. The present ML model was applied to design a new promising cutting condition which exhibited a good cutting efficiency. The model is thus applicable in both predicting and optimizing the tool performance for Inconel 718 face milling real operation, demonstrating the potential contribution to the intelligent manufacturing systems according to industry 4.0.

2 Methodology

2.1 Materials and machining process

Inconel 718 was purchased from Jiangsu DZX Technology Company Co., Ltd, China. Surface milling of Inconel 718 was carried out on a 14 kW DMC 835 V-DECKEL MAHO CNC vertical milling machine using the down-milling operation, where a 4-bar mineral oil–based (85% mineral oil and 15% additives) flood coolant was applied to minimize heat and friction on the tool-workpiece contact zone during machining. Multi-layer PVD-TiAlN/NbN-coated inserts

manufactured by SECO Tools, Sweden, with a cutter designation of R220.53–0032-09-4A arbor mounting, were used in the machining process. Four inserts were installed onto the cutter for the machining process, as shown in Fig. 1. Details of Inconel 718, cutting tools, and machining process can be found in supplementary information (SI) Section S1.

2.2 Data collection

The flow chart of the research process is summarized in Fig. 1. The first step involved VB data collection during experiments. This step included a full factorial design of experiment (DoE), and VB measurement. Table 1 summarizes the DoE applied in this research (see details in SI section S1). The cutting conditions varied in terms of cutting speed (V_c), feed rate (f_r), and ADOC (a_p). Data were collected at 200 to 400 mm cutting length intervals. After cutting with a given cutting length interval, the cutting tools were removed from the cutter and placed onto an optical microscope (Olympus U-MSSP4, BX53M, 1000× magnification, Tokyo, Japan) for VB measurement on the flank face of the cutting edge. VB of 500 μm was set as the failure criterion of tools based on the ISO 8688–1 standard to determine the maximum tool life in this research and it was also used in [31]. The experimental measurement error of VB was 0.58 μm. The machining process was stopped when any of the four cutting inserts reached or exceeded the criterion of 500 μm. VB data used in the ML model training

was thus the average value of the four inserts. The average and standard deviation of the measured VB was 223.6 and 174 μm, respectively.

2.3 Machine learning modeling

The second step of the current research was to develop the ML model based on the VB data collected. The ML model used in this study was the GKRR model, which is a ridge regression–type ML model with a radial basis function, as shown in Eq. (1). Radial basis function determines the distance between feature vectors x_i and x_j :

$$k_{ij} = \exp(-\gamma \|x_i - x_j\|^2) \tag{1}$$

where γ is a hyperparameter that represents the length scale between two given features. The loss function for training the GKRR ML model is shown in Eq. (2):

$$\text{Loss function} = \|Y - K\beta\|_2^2 + \alpha\beta^T K\beta \tag{2}$$

where Y is the target feature, K is the Gaussian kernel, β is the coefficient, and α is the coefficient of the L2-norm penalty used to penalize the fitting coefficients. The input features were cutting speed, feed rate, ADOC, and cutting length. The output feature was VB. Table 2 tabulates the statistics of each feature. The data set used in the study consists of the experimentally measured VB data as well as the boundary condition data. The boundary condition data was

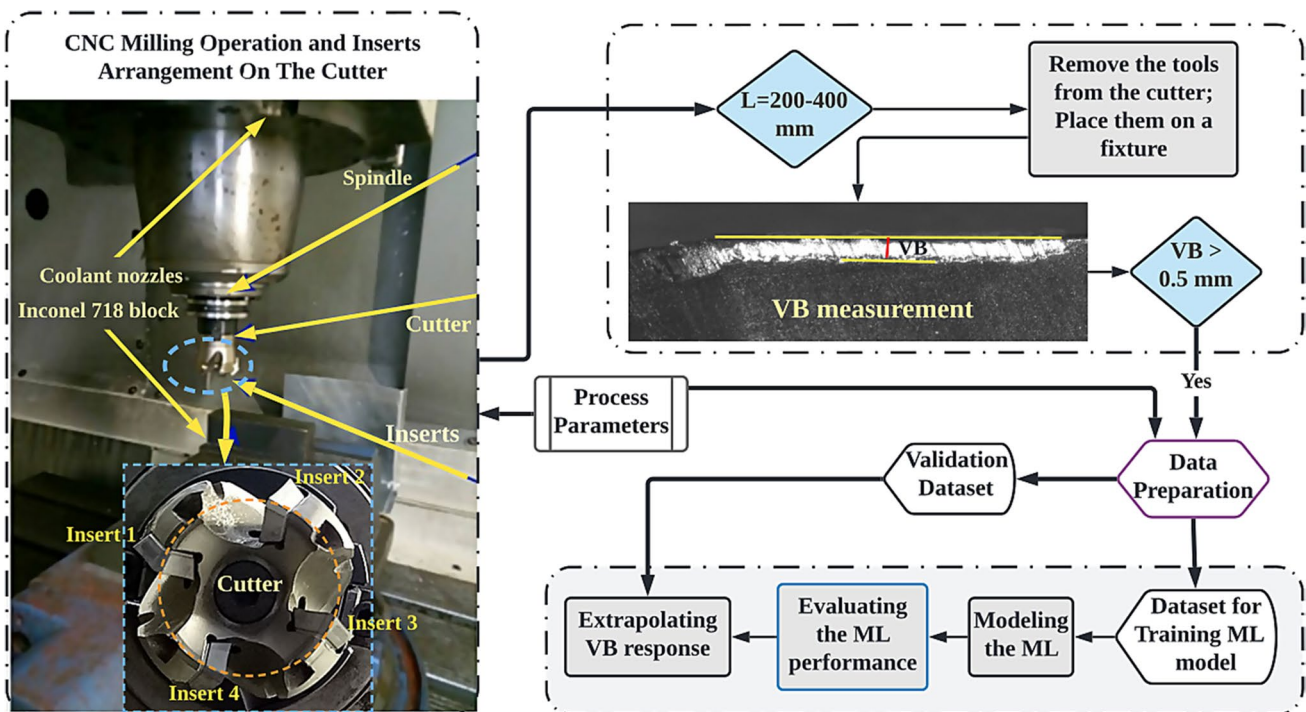


Fig. 1 Flow chart of the research methodology

Table 1 The full factorial design of experiment

Experimental run	Cutting speed (V_c) (m/min)	Feed rate (f_t) (mm/tooth)	Axial depth of cut (a_p) (mm)
1	40	0.07	0.5
2	40	0.07	0.75
3	40	0.07	1
4	40	0.1	0.5
5	40	0.1	0.75
6	40	0.1	1
7	40	0.13	0.5
8	40	0.13	0.75
9	40	0.13	1
10	60	0.07	0.5
11	60	0.07	0.75
12	60	0.07	1
13	60	0.1	0.5
14	60	0.1	0.75
15	60	0.1	1
16	60	0.13	0.5
17	60	0.13	0.75
18	60	0.13	1
19	80	0.07	0.5
20	80	0.07	0.75
21	80	0.07	1
22	80	0.1	0.5
23	80	0.1	0.75
24	80	0.1	1
25	80	0.13	0.5
26	80	0.13	0.75
27	80	0.13	1

introduced in order to force the ML model to have correct performance at the conditions where VB should be zero. These conditions refer to the ones at zero cutting speed, feed rate, ADOC, and/or cutting length inputs. The total data were 740, which included 137 experimentally determined and 603 boundary condition data. The hyperparameters (α , γ) of the ML model were optimized using a genetic algorithm (GA) with a custom cost function taking the leave out (LO) group cross-validation (CV) average root mean square error

(RMSE) as the scoring metric. A set of data with the same cutting speed, feed rate, and ADOC was considered a group. In a given group, cutting length remained as variables. For instance, cutting speed = 80 m/min, feed rate = 0.07 mm/tooth, and ADOC = 1 mm with cutting length ranging from 400 to 1200 mm were one group. The model analysis and exploration were primarily performed with the MAterials Simulation Toolkit for Machine Learning (MAST-ML) [32], an open-source Python package with scikit-learn [33] library to automate ML workflows and model assessments. A 5-fold CV and cross-plot analyses were carried out to assess the model. The 5-fold CV test was repeated 20 times in this work, and the CV RMSE was given as the average of the fold-average RMSEs. Details of the CV methods and the cross-plot analyses can be found elsewhere [27].

2.4 Characterization of wear mechanism

When VB of a given inserts exceeded the failure criterion (i.e., 500 μm), tools were soaked in hydrogen chloride acid and placed in an ultrasonic bath for 15 min to remove the Inconel 718 adhesive particles and wear debris. Then, they were soaked again in acetone and placed in the ultrasonic bath for 10 min to remove the remaining acid on the tool's cutting edge. Field-emission scanning electron microscope (FESEM, FEI Quanta 400 F, USA) was primarily used in observing dominant failure modes and wear mechanisms of the tools. Tool samples were mounted on metal stubs with carbon adhesive tape, oriented at 45° angle, allowing FESEM to view the insert's cutting edge.

3 Results and discussion

3.1 Machine learning model analysis

3.1.1 Cross plots

Model evaluation from full-fit (RMSE = 30.9 μm and $R^2 = 0.93$) and 5-fold CV test (RMSE = 49.7 μm and $R^2 = 0.81$) suggested that the model had some predictive ability (see details in SI section S2). We further evaluated the fitting quality by using cross-plot analysis, which visualizes

Table 2 The statistics of each feature used in the present study

Feature	Maximum	Minimum	Average	Standard deviation	Unit
Flank wear (VB)	674	0	41.4	114.5	μm
Cutting speed (V_c)	100	0	41.0	27.5	m/min
Feed rate (f_t)	0.15	0	0.07	0.05	mm/tooth
Axial depth of cut (a_p)	1.5	0	0.6	0.4	mm
Cutting length (L)	5400	0	1179	1199	mm

the relationship between multi-variables. Figures 2, 3, and 4 show the cutting length cross plots at cutting speed of 40, 60, and 80 m/min, respectively. Values in parenthesis, i.e., (X,Y,Z), shown in the each plot represents cutting speed, feed rate, ADOC, respectively, which were held as constant variables when performing the cross-plot analysis. For instance, (40, 0.07, 0.5) shown in Fig. 2 represents that cutting speed of 40 m/min, feed rate of 0.07 mm/tooth, and ADOC of 0.5 mm were held and we observed VB profile in terms of cutting length. The scattered point and the solid line in the plot represent the measured VB data and ML predicted VB data, respectively.

In general, all the predicted data agreed well with the measured one. At the lowest cutting speed of 40 m/min and the lowest feed rate of 0.07 mm/tooth (Fig. 2), the VB profile exhibited three stages—(1) rapid VB formation due to break-in of the tools when cutting initializes, (2) a slow increase in VB in the middle of the cutting length due to minimum plastic deformation and wear mechanisms, and (3) a rapid

increase in VB due to unprecedented wear mechanisms as the tools approach the failure criteria. This profile seems consistent with the literature finding that flank wear evolves in three stages, namely early rapid wear, uniform wear, and failure region [10]. While increasing the feed rate from 0.07 to 0.13 mm/tooth, the abovementioned stage 2 gradually vanished. In this case, VB accelerated into the rapid failure region after the initial break-in, indicating a high tool deterioration rate caused by severe wear mechanisms and failure modes. Similar VB profiles are found in Figs. 3 and 4. When the cutting speed was increased to 80 m/min (Fig. 4), all the VB profiles exhibited the type in which only stage 1 and stage 3 existed even at the lowest feed rate. These profiles suggest that face milling of Inconel 718 at such a high speed would cause severe unprecedented wear mechanisms and failure modes on the tool’s cutting edge, which was not feasible for real applications. This viewpoint is consistent with literature findings, but this is the first time that a quantitative VB profile of PVD-TiAlN/NbN-coated carbide tools was

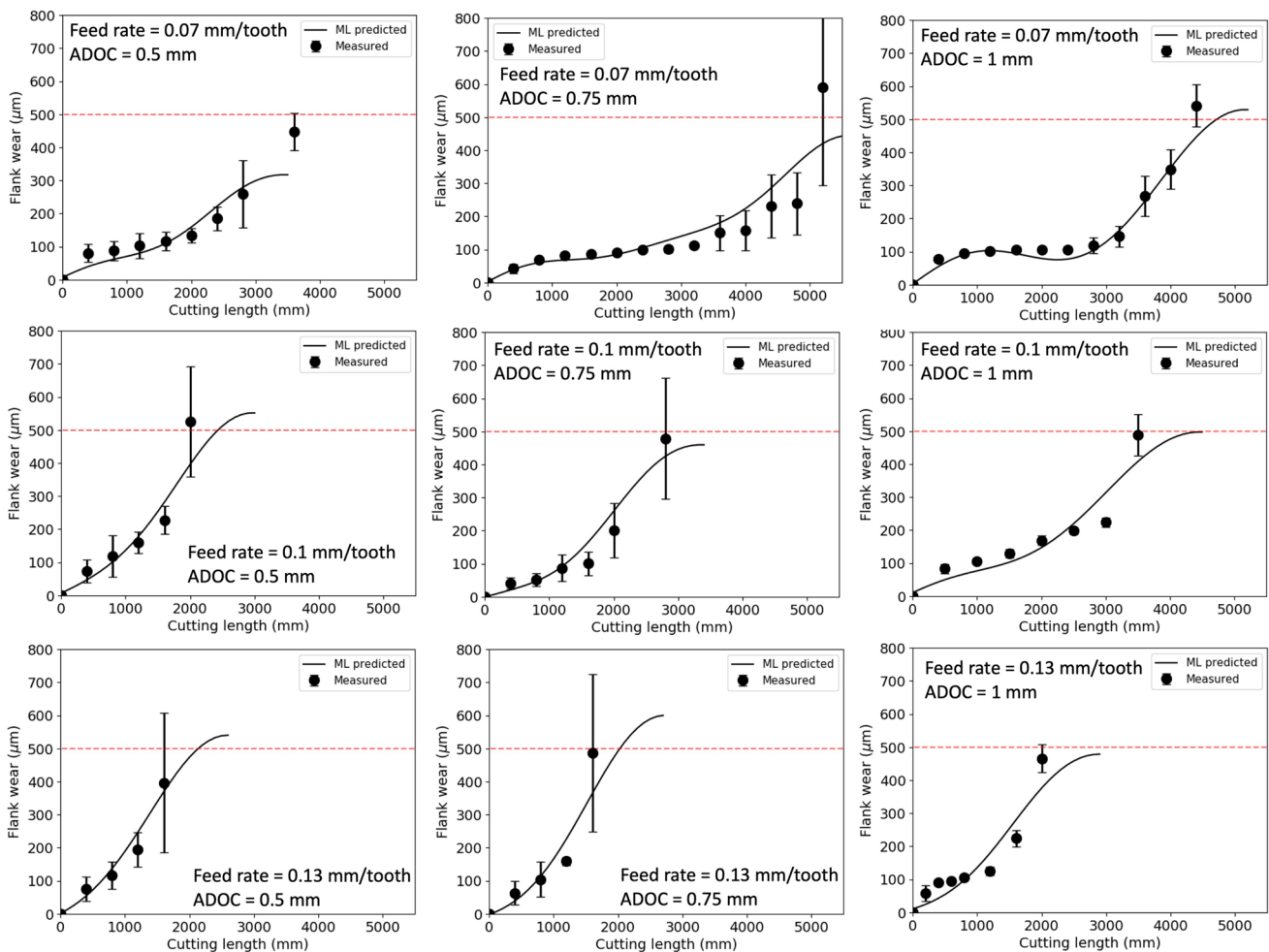


Fig. 2 Cutting length cross plot at cutting speed=40 m/min. The error bar shown in the plots was the standard deviation of VB from the four inserts. The red dotted line represents VB criteria of 500 µm based on ISO 8688–1 standard

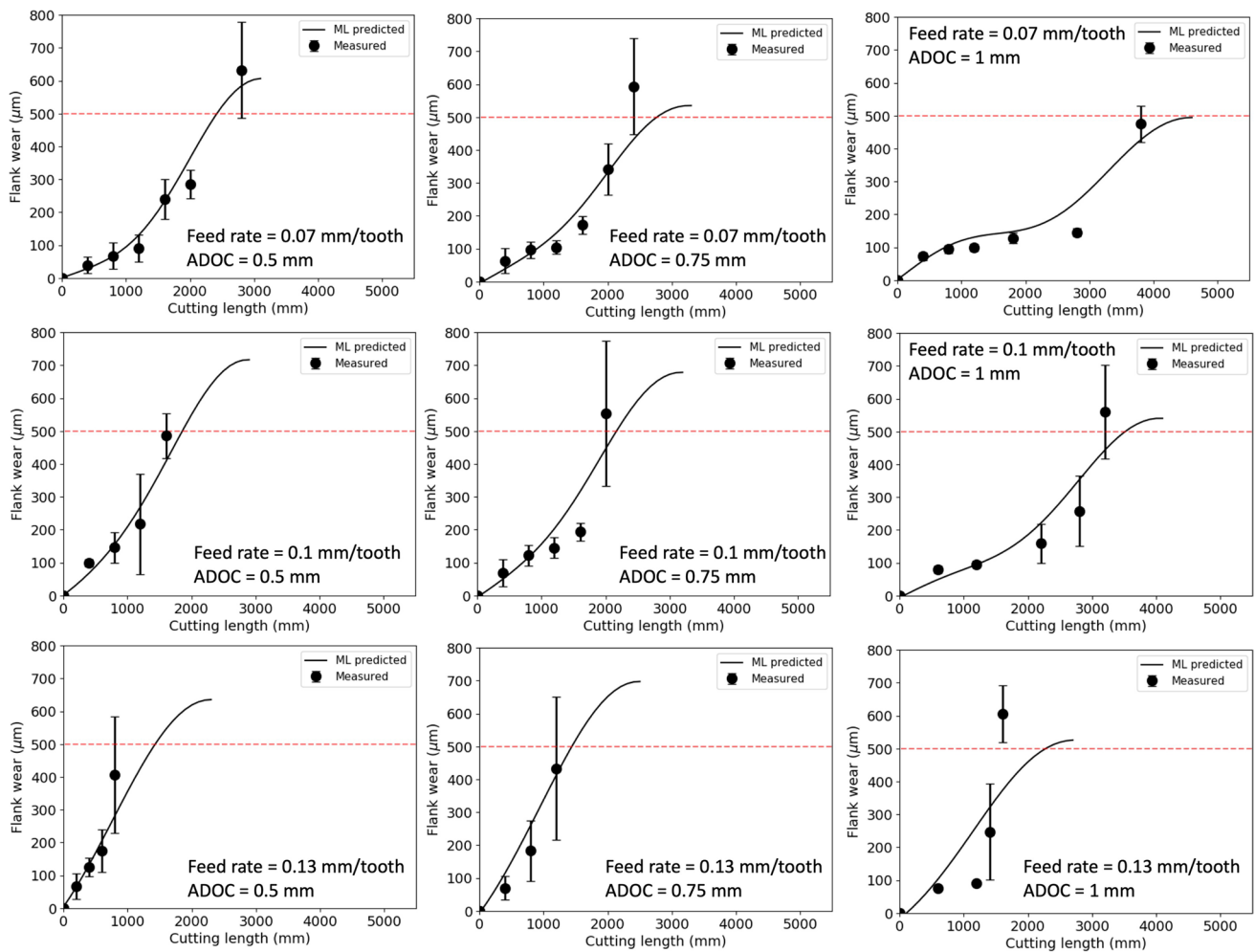


Fig. 3 Cutting length cross plot at cutting speed=60 m/min. The error bar shown in the plots was the standard deviation of VB from the four inserts. The red dotted line represents VB criteria of 500 μm based on ISO 8688–1 standard

possible in terms of the multiple cutting parameters. A more detailed mechanistic study of these VB profiles is pursued in our ongoing projects.

3.1.2 VB contour diagram

It has been pointed out that when ADOC was less than 0.75 mm, a more localized chipping on the depth of cut (DOC) line was caused due to a high shear force on the precipitation-hardened layer. It is thus we selected a new ADOC condition at 0.9 mm to plot the VB contour diagram at various cutting speed, feed rate, and cutting length. Figure 5 a to f show the VB contour diagrams at cutting speed of 30, 40, 50, 60, 70, and 80 m/min, respectively. The red hollow circle represents $\text{VB} < 500 \mu\text{m}$ at the given cutting condition. The black solid line represents the cutting time in the unit of minutes. The blue solid line represents the removed depth from the cutting process in the unit of millimeter. The convenience of the VB contour diagram is

to visualize the promising cutting condition space where the minimum VB, minimum cutting time, and maximum removed depth could be achieved. For instance, at ADOC of 0.9 mm, cutting speed of 30 m/min, and feed rate of 0.1 mm/tooth, removed depth of 50 mm with cutting time of ca. 60 min was required and VB was less than the 500 μm criteria. On contrary, at ADOC of 0.9 mm, cutting speed of 80 m/min, and feed rate of 0.05 mm/tooth, removed depth of < 15 mm and VB exceeded the 500 μm criteria. In the following section, we will discuss a promising designed cutting condition from this contour diagram and performed an experiment for validation.

3.1.3 Promising cutting condition design, validation, and its wear mechanisms

Based on the contour property plot shown in Fig. 5, we designed a promising cutting condition at cutting speed of 40 m/min, feed rate of 0.08 mm/tooth, and ADOC of

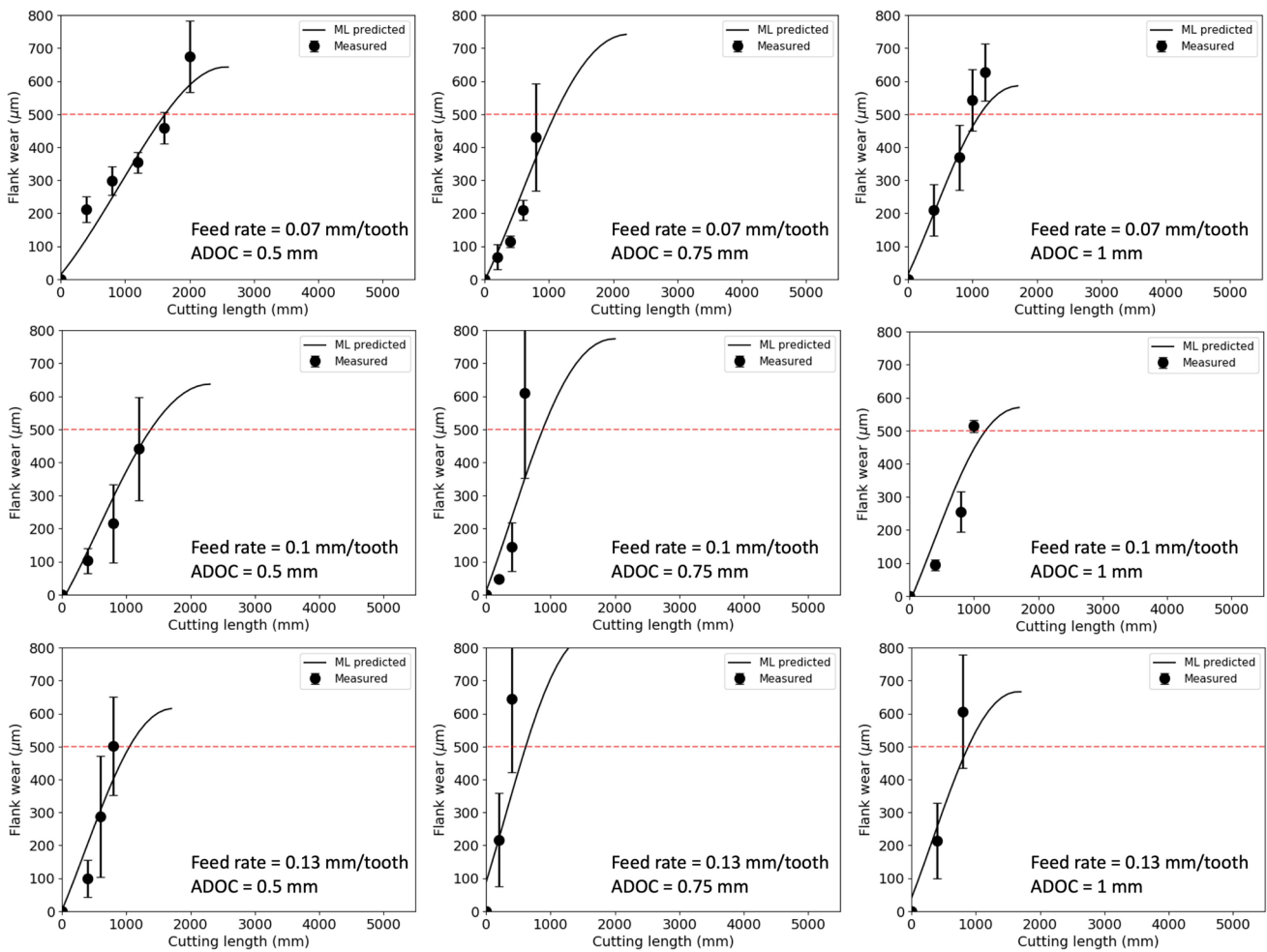


Fig. 4 Cutting length cross plot at cutting speed = 80 m/min. The error bar shown in the plots was the standard deviation of VB from the four inserts. The red dotted line represents VB criteria of 500 µm based on ISO 8688–1 standard

0.9 mm because the ML model predicted that cutting at this condition can yield a high tool performance, achieving the cutting depth of 43 mm within 50 min before VB reached 500 µm. A parallel experiment was performed to validate the designed cutting condition. Figure 6 shows the VB progression with respect to the cutting length diagram. The scattered points are the measured VB while the solid line is the ML predicted VB. There were some discrepancies between the measured and the predicted data. Before the cutting length of 3000 mm, the prediction was underestimated, while after that, the prediction was overestimated. It was until cutting length of 4400 mm that the prediction agreed well with the measured one. Although there was an error of ca. 100 µm at cutting length of 4000 mm, overall, these errors were considered minor. In general, the model could capture the VB progression profile at an unknown cutting condition. The model could also capture the correct cutting length to reach the 500 µm criteria. We believed the model was able to capture this condition because in

the vicinity there was data at cutting speed of 40 m/min, feed rate of 0.07 mm/tooth, ADOC of 1 mm, and cutting length of 4400 mm. The measured VB, removed depth, and time at this condition were 540.8 µm, 44 mm, and 51.7 min, respectively. After the experimental validation, we confirmed that the newly designed cutting condition yielded a removed depth of 42 mm with 47 min and VB reached 551 µm.

Figure 6 shows that there were also three stages of VB progression from low to high cutting length. These three stages may attribute to early rapid wear, uniform wear, and failure region. It seems thus straightforward to further study the wear mechanism underlying the design cutting condition. Figure 7 shows the microstructure of the tool’s cutting edge after facing milling up to 4600 mm cutting length. Figure 7a shows the optical micrograph of the tool exhibiting the uniform flank wear at cutting length of 1200 mm. When the cutting length reached 4000 mm, a progressive chipping occurred in the failure region as

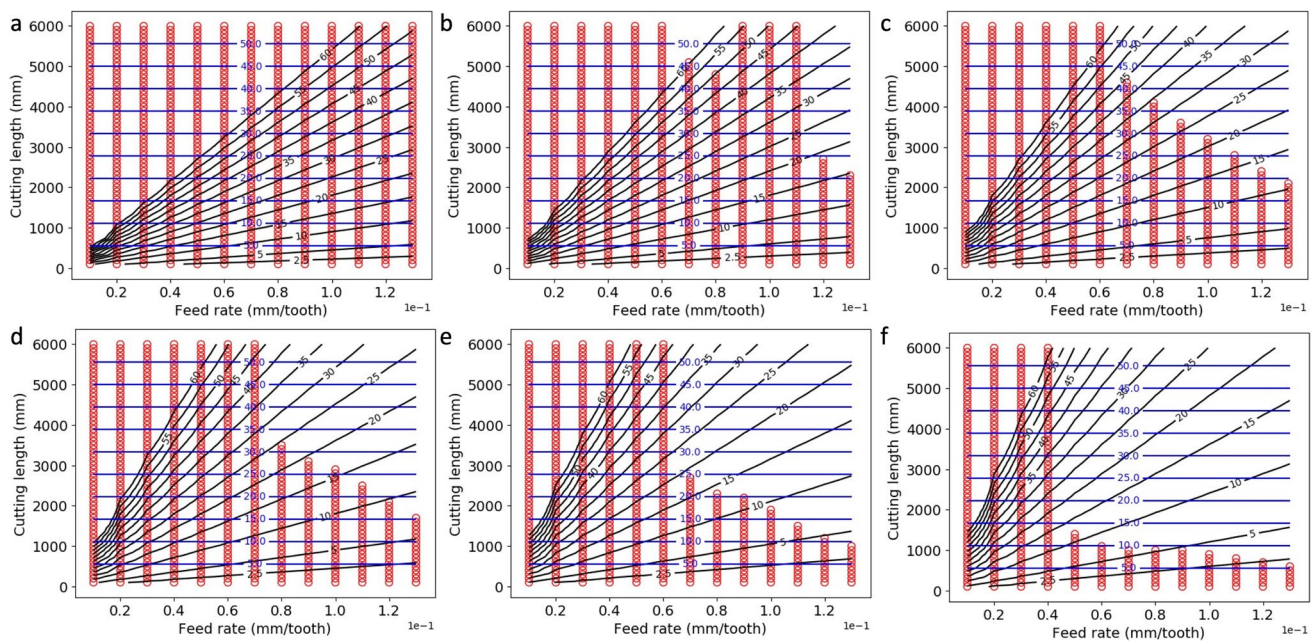


Fig. 5 Cutting length vs. feed rate plot at AD0C of 0.9 mm and cutting speed of (a) 30, (b) 40, (c) 50, (d) 60, (e) 70, and (f) 80 m/min. The red hollow circle represents $VB < 500 \mu\text{m}$ at the given cutting

condition. The black solid line represents the cutting time in the unit of minutes. The blue solid line represents the removed depth from the cutting process in the unit of millimeter

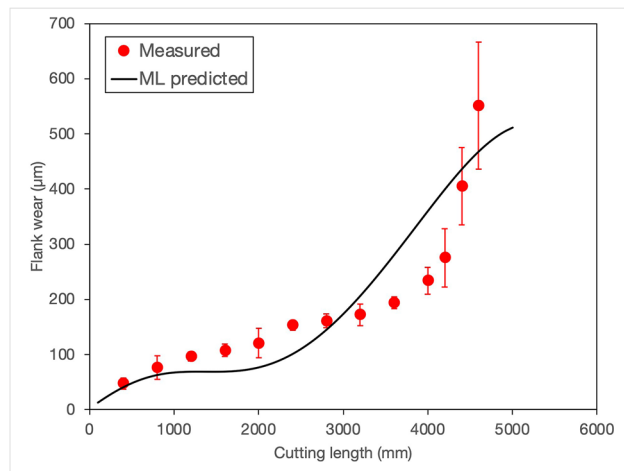


Fig. 6 Validation at the cutting condition of AD0C=0.9 mm, feed rate=0.08 mm/tooth, and cutting speed=40 m/min. The red solid circle represents the measured VB which did not include in the training data set. The error bar shown in the plots was the standard deviation of VB from the four inserts. The black solid line represents the ML predicted VB

shown in Fig. 7b. It was attributed to synergistic effect of abrasion and cyclic adhesion on the tool's cutting edge [11]. BUE or built-up layer (BUL) formation accelerated progressive chipping as BUE got plucked by the subsequent cut [34], as shown in Fig. 7c and d, when the cutting length reached 4400 and 4600 mm, respectively. The

small chip load also reduced the cutting force and cyclic adhesion by BUE or BUL formation. Figure 7e and f show secondary electron image (SEI) of the dotted-line region in Fig. 7c and d, respectively. The microstructure revealed that the localized chipping in the failure region was caused by abrasion and cyclic adhesion.

At AD0C of 0.9 mm, the tools cut a large workpiece depth free from precipitation hardening layer, thereby minimizing the severe abrasion that caused progressive chipping and mechanical cracks [34]. In addition, a low cutting speed also caused low temperature and stresses, reducing chip deformation, and producing a thin BUL layer that stuck to the flank wear region [35]. Moreover, BUL at the lowest speed experienced negligible precipitation hardening effect due to low cutting temperature. Therefore, cutting at a low speed of 40 m/min led to a low adhesive strength that caused less tool particles removed together with the BUL in the subsequent passes, minimizing chipping and flaking of the tool's flank face [15]. On the other hand, the lowest feed rate, less than 0.08 mm/tooth, minimized the chip load that caused high friction force, rubbing action, and abrasion on the tool's cutting edge [36]. Even though the present ML model was not informed by any microstructure information, the fact that the model could predict a promising cutting condition in minimizing the rapid VB progression was quite remarkable. It is also worth noted that the present study used only a small data set, including only 137 experimentally determined data. The

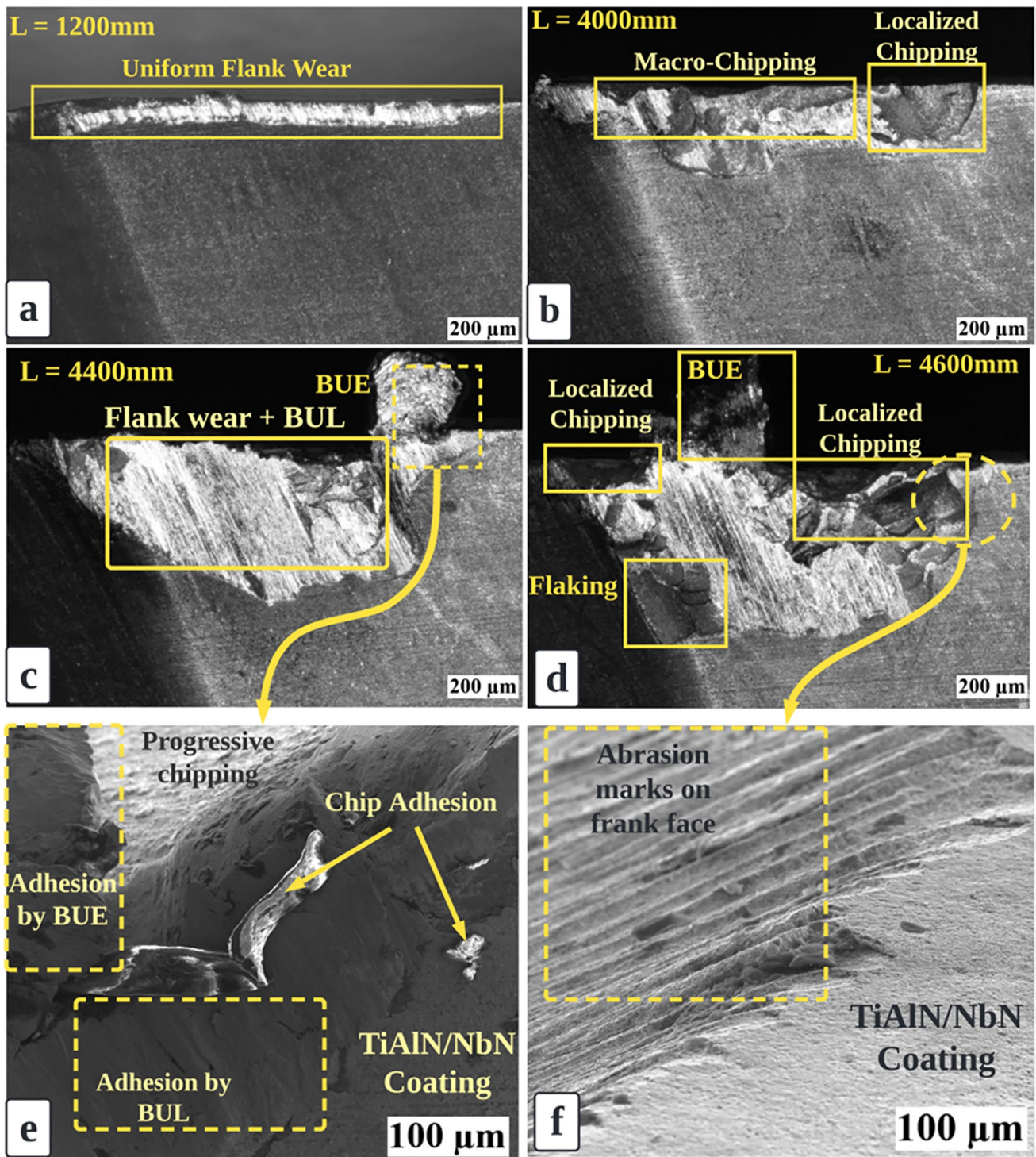


Fig. 7 Optical micrograph of TiAlN/NbN-coated carbides inserts at 40 m/min, 0.08 feed/tooth, and 0.9 mm ADOC after cutting length of (a) 1200, (b) 4000, (c) 4400, and (d) 4600 mm. Secondary electron

images of the dotted-line region in (c) and (d) showing the localized chipping caused by abrasion and cyclic adhesion after cutting length of (e) 4400 and (f) 4600 mm

success of the cutting condition design suggests the power and potential in using ML modeling method to predict and optimize VB progression during face milling of Inconel 718 for real applications.

4 Conclusion

This research employed the GKRR ML method to develop the VB prediction model for face milling Inconel 718 using

TiAlN/NbN-coated carbide inserts with the input feature of cutting speed, feed rate, ADOC, and cutting length. The model showed a RMSE of 30.9 (49.7) μm and R^2 of 0.93 (0.81) in full fit (5-fold CV test). The statistics along with the cross-plot analyses suggested that the model had some predictive ability. The model captured the correct VB profile evolution although it was not informed by any microstructure information. These profiles were consistent with the existing findings which qualitatively suggest the early rapid wear, uniform wear, and failure regions, whereas this study provides a quantitative VB progression prediction. The present ML model was further applied to extrapolate to unknown cutting conditions. A new promising condition at cutting speed of 40 m/min, feed rate of 0.08 mm/tooth, and ADOC of 0.9 mm was designed. The designed cutting condition was experimentally validated. When the cutting length reached 4000 mm, a progressive chipping occurred in the failure region based on the microstructure analysis. The designed condition yielded a removed depth of 42 mm for 47 min with VB of 551 μm . The measured and predicted VB agreed well with each other. The complexity of the present ML model primarily includes predicting VB in a high dimensional space where the practical processing parameters of cutting speed, feed rate, ADOC, and cutting length were used. Even though the present ML model was only informed by the cutting conditions with a small amount of data, it can predict correct VB, and deciphering its complex physics. This model is thus believed applicable in real face milling operation of Inconel 718, demonstrating the potential contribution to the intelligent manufacturing systems, including tool performance prediction, control, and optimization, according to industry 4.0.

Supplementary Information The online version contains supplementary material available at <https://doi.org/10.1007/s00170-023-11152-3>.

Author contribution All authors contributed to the conceptual idea of the manuscript. The first draft of the manuscript was written by Mr. Tiyamike Banda and Dr Yu-chen Liu. All authors commented on the previous versions. Dr. Yu-chen Liu, Dr. Ali Akhavan Farid, and Dr. Chin Seong Lim supervised, reviewed, and edited the manuscript. All authors read and finally approved the final version of the manuscript.

Funding This work was supported by the National Science and Technology Council (NSTC) (110-2222-E-006-008, 111-2222-E-006-011-MY3, and 111-2622-8-006-029) and from the Featured Areas Research Center Program within the framework of the Higher Education Sprout Project by the Ministry of Education (MOE) and NSTC (111-2634-F-006-008) in Taiwan.

Data availability The data used in this manuscript is available from the corresponding author and can be accessed on reasonable request.

Code availability Not applicable.

Declarations

Ethics approval Not applicable because this article does not contain any studies with human or animal subjects.

Consent to participate Not applicable.

Consent for publication Not applicable.

Conflict of interest The authors declare no competing interests.

References

1. Arunachalam RM, Mannan MA, Spowage AC (2004) Surface integrity when machining age hardened Inconel 718 with coated carbide cutting tools. *Int J Mach Tools Manuf* 44(14):1481–1491. <https://doi.org/10.1016/j.ijmactools.2004.05.005>
2. Dudzinski D, Devillez A, Moufki A, Larrouquère D, Zerrouki V, Vigneau J (2004) A review of developments towards dry and high speed machining of Inconel 718 alloy. *Int J Mach Tools Manuf* 44(4):439–456. [https://doi.org/10.1016/S0890-6955\(03\)00159-7](https://doi.org/10.1016/S0890-6955(03)00159-7)
3. Chan CH et al (2017) Analysis of face milling performance on Inconel 718 using FEM and historical data of RSM. *IOP Conf Ser Mater Sci Eng* 270(1). <https://doi.org/10.1088/1757-899X/270/1/012038>
4. Houghton Q (n.d.) Quaker Houghton - industrial chemicals, process fluids & lubricants. https://home.quakerhoughton.com/?utm_source=quakerchem&utm_medium=Legacy&utm_campaign=Decommissioning&utm_term= Accessed 02 Apr 2022
5. Polvorosa R, Suárez A, López de Lacalle LN, Cerrillo I, Wretland A, Veiga F (2017) Tool wear on nickel alloys with different coolant pressures: comparison of Alloy 718 and Waspaloy. *J Manuf Process* 26:44–56. <https://doi.org/10.1016/j.jmapro.2017.01.012>
6. Akhtar W, Sun J, Sun P, Chen W, Saleem Z (2014) Tool wear mechanisms in the machining of Nickel based super-alloys: a review. *Front Mech Eng* 9(2):106–119. <https://doi.org/10.1007/s11465-014-0301-2>
7. Kamdani et al (2019) Study on tool wear and wear mechanism of end milling Nickel-based alloy. *Jurnal Tribologi* 2019(21):82–92
8. Banda T, Ho KY, Akhavan Farid A, Lim CS (2021) Characterization of tool wear mechanisms and failure modes of TiAlN-NbN coated carbide inserts in face milling of Inconel 718. *J Mater Eng Perform*. <https://doi.org/10.1007/s11665-021-06301-2>
9. Anderson M, Patwa R, Shin YC (2006) Laser-assisted machining of Inconel 718 with an economic analysis. *Int J Mach Tools Manuf* 46(14):1879–1891. <https://doi.org/10.1016/j.ijmactools.2005.11.005>
10. Huang W et al (2021) Tool wear in ultrasonic vibration-assisted drilling of CFRP: a comparison with conventional drilling. *Int J Adv Manuf Technol* 1809–1820. <https://doi.org/10.1007/s00170-021-07198-w>
11. Ezugwu EO, Wang ZM, Machado AR (2000) Wear of coated carbide tools when machining nickel (Inconel 718) and titanium base (Ti-6Al-4V) alloys. *Tribol Trans* 43(2):263–268. <https://doi.org/10.1080/10402000008982338>
12. Liu Y, Yu S, Shi Q, Ge X, Wang W (2022) Multilayer coatings for tribology: a mini review. *Nanomaterials* 12:1388. <https://doi.org/10.3390/nano12091388>
13. Jawaid A, Koksai S, Sharif S (2001) Cutting performance and wear characteristics of PVD coated and uncoated carbide tools in face milling Inconel 718 aerospace alloy. *J Mater Process Technol* 116(1):2–9. [https://doi.org/10.1016/S0924-0136\(01\)00850-0](https://doi.org/10.1016/S0924-0136(01)00850-0)
14. Suresh R, Basavarajappa S, Gaitonde VN (2015) Experimental studies on the performance of multilayer coated carbide tool in hard turning of high strength low alloy steel. *J Mater Res* 30(20):3056–3064. <https://doi.org/10.1557/jmr.2015.236>
15. Anthony Xavier M, Manohar M, Madhukar PM, Jeyapandiarajan P (2017) Experimental investigation of work hardening,

- residual stress and microstructure during machining Inconel 718. *J Mech Sci Technol* 31(10):4789–4794. <https://doi.org/10.1007/s12206-017-0926-2>
16. Klocke F, Lung D, Cordes SE, Gerschwiler K (2008) Performance of PVD-coatings on cutting tools for machining Inconel 718, austenitic steel and quenched and tempered steel. *Proceedings of the 7th International Conference THE Coatings in Manufacturing*, no. October
 17. Kosaraju S, Vijay Kumar M, Sateesh N (2018) Optimization of machining parameter in turning Inconel 625. *Mater Today: Proceedings* 5(2): Part 1, 5343–5348. <https://doi.org/10.1016/j.matpr.2017.12.119>
 18. Guo J, Li A, Zhang R (2020) Tool condition monitoring in milling process using multifractal detrended fluctuation analysis and support vector machine. *Int J Adv Manuf Technol* 110(5):1445–1456. <https://doi.org/10.1007/s00170-020-05931-5>
 19. Banda T, Farid AA, Li C, Jawu VL, Lim CS (2022) Application of machine vision for tool condition monitoring and tool performance optimization—a review. *Int J Adv Manuf Technol* 121(11):7057–7086. <https://doi.org/10.1007/s00170-022-09696-x>
 20. Gao D, Liao Z, Lv Z, Lu Y (2015) Multi-scale statistical signal processing of cutting force in cutting tool condition monitoring. *Int J Adv Manuf Technol* 80(9–12):1843–1853. <https://doi.org/10.1007/s00170-015-7116-0>
 21. Thakre AA, Lad AV, Mala K (2019) Measurements of tool wear parameters using machine vision system. *Model Simul Eng* 2019:1–10. <https://doi.org/10.1155/2019/1876489>
 22. Salimiasl A, Özdemir A (2016) Analyzing the performance of artificial neural network (ANN)-, fuzzy logic (FL)-, and least square (LS)-based models for online tool condition monitoring. *Int J Adv Manuf Technol* 87(1–4):1145–1158. <https://doi.org/10.1007/s00170-016-8548-x>
 23. Morgan D, Jacobs R (2020) Opportunities and challenges for machine learning in materials science. *Annu Rev Mater Res* 50:71–103. <https://doi.org/10.1146/annurev-matsci-070218-010015>
 24. Link P et al (2022) Capturing and incorporating expert knowledge into machine learning models for quality prediction in manufacturing. *J Intell Manuf* 2022:1–14. <https://doi.org/10.1007/S10845-022-01975-4>
 25. Liu YC, Afflerbach B, Jacobs R, Lin SK, Morgan D (2019) Exploring effective charge in electromigration using machine learning. *MRS Commun* 9(2):567–575. <https://doi.org/10.1557/mrc.2019.63>
 26. Liu YC, Liu TY, Huang TH, Chiu KC, Lin SK (2021) Exploring dielectric constant and dissipation factor of ltcc using machine learning. *Materials* 14(19):1–14. <https://doi.org/10.3390/ma14195784>
 27. Liu Y-c, Wu H, Mayeshiba T et al (2022) Machine learning predictions of irradiation embrittlement in reactor pressure vessel steels. *NPJ Comput Mater* 8:85. <https://doi.org/10.1038/s41524-022-00760-4>
 28. Wu X, Liu Y, Zhou X, Mou A (2019) Automatic identification of tool wear based on convolutional neural network in face milling process. *Sensors (Switzerland)* 19(18). <https://doi.org/10.3390/s19183817>
 29. Kaya B, Oysu C, Ertunc HM (2011) Advances in Engineering Software Force-torque based on-line tool wear estimation system for CNC milling of Inconel 718 using neural networks. *Adv Eng Softw* 42(3):76–84. <https://doi.org/10.1016/j.advengsoft.2010.12.002>
 30. Nath C, Brooks Z, Kurfess TR (2015) Machinability study and process optimization in face milling of some super alloys with indexable copy face mill inserts. *J Manuf Process* 20:88–97. <https://doi.org/10.1016/j.jmapro.2015.09.006>
 31. Banda T, Lestari V, Chuan J, Ali L, Farid A, Seong C (2022) Flank wear prediction using spatial binary properties and artificial neural network in face milling of Inconel 718. *Int J Adv Manuf Technol* 0123456789. <https://doi.org/10.1007/s00170-022-09039-w>
 32. Jacobs R et al (2020) The Materials Simulation Toolkit for Machine learning (MAST-ML): an automated open source toolkit to accelerate data-driven materials research. *Comput Mater Sci* 176:2019. <https://doi.org/10.1016/j.commatsci.2020.109544>
 33. Pedregosa F et al (2011) Scikit-learn: machine learning in Python. *J Mach Learn Res* 12(2014):2825–2830
 34. De Melo ACA, Milan JCG, Da Silva MB, Machado ÁR (2006) Some observations on wear and damages in cemented carbide tools. *J Braz Soc Mech Sci Eng* 28(3):269–277. <https://doi.org/10.1590/s1678-58782006000300004>
 35. Bilgin MB (2015) Investigating the effects of cutting parameters on the built-up-layer and built-up-edge formation during the machining of AISI 310 austenitic stainless Steels. *Materiali Tehnologije* 49(5):779–784. <https://doi.org/10.17222/mit.2014.253>
 36. Kakaš D et al (2009) Influence of load and sliding speed on friction coefficient of IBAD deposited TiN. *Tribol Ind* 31(3–4):3–10

Publisher's note Springer Nature remains neutral with regard to jurisdictional claims in published maps and institutional affiliations.

Springer Nature or its licensor (e.g. a society or other partner) holds exclusive rights to this article under a publishing agreement with the author(s) or other rightsholder(s); author self-archiving of the accepted manuscript version of this article is solely governed by the terms of such publishing agreement and applicable law.